

324-34
82257

Dynamics of the Molten Contact Line

Ain A. Sonin and Stefano Schiaffino

Department of Mechanical Engineering
Massachusetts Institute of Technology
Cambridge, MA 02139

A great deal of work has been published on the capillarity-driven motion of an ordinary liquid over a solid surface (the *isothermal* dynamic contact line problem). The solution to this problem may be stated in terms of a functional relationship between the contact line speed U , the dynamic contact angle θ , and the relevant properties of the system's three phases and their interfaces. One such relationship is the much-quoted empirical correlation of Hoffman (1975), who showed that for $Ca = \mu U / \sigma < 1$, where μ is the liquid viscosity and σ the surface tension, a large amount of data spanning many orders of magnitude in Ca could be correlated approximately by the formula $Ca = k(\theta^3 - \theta_e^3)$, where θ_e is the equilibrium contact angle and $k \approx 0.013$. On the theoretical side, the continuum theory of the moving contact line contains the well-known non-integrable shear stress singularity at the contact line [e.g. Tanner (1979), de Gennes (1985, 1990), Cox (1986), Leger (1992)]. The singularity can be removed by specifying a velocity slip model or cut-off very close to the contact line [e.g. Huh (1971, 1977), Dussan V. (1974, 1976, 1979, 1991), Durbin (1988), Haley (1991), Hocking (1992)], and the parameters can be chosen so as to yield agreement with experiment [Fermigier (1991), Chen (1992), Leger (1992)]. An entirely different theory for the dynamic contact line has been put forward by Blake (1969) based on Eyring's reaction rate theory for liquids. With an appropriate selection of physical parameters, this molecular-kinetic theory can also be brought into agreement with experimental data [Blake (1969, 1979, 1994), Gribanova (1992)]. Some progress has also been made recently in applying molecular-dynamic computations to the contact line (Thompson et al, 1993; Koplic & Banavar, 1995), but these are limited to mesoscale systems. Clearly, despite the large amount of work, this problem is not yet conclusively resolved.

In contrast to the ordinary contact line problem, virtually no information is available on the similar problem associated with a *molten* material spreading on a solid which is below the melt's fusion point. The latter is a more complex problem in which heat transfer and solidification take place simultaneously with spreading, and requires answers not only for the hot melt's advance speed over the cold solid as a function of contact angle, but also for how one is to predict the point of the molten contact line's arrest by freezing. These issues are of importance in evolving methods of materials

processing. For example, finely featured components can be fabricated under computer control by precise deposition of individual molten microdrops, each droplet solidifying by heat loss after it lands (Gao & Sonin, 1994). In this case, the point of a droplet's contact line arrest will control its post-deposition solid shape, that is, the shape of the basic microscale "building block" of the process.

The purpose of our work is to develop, based on both experiments and theory, an understanding of the dynamic processes that occur when a molten droplet touches a subcooled solid, spreads partly over it by capillary action, and freezes. We seek answers to the following basic questions. First, what is the relationship between the melt's contact line speed and the apparent (dynamic) contact angle? Secondly, at what point will the contact line motion be arrested by freezing?

A simple well-defined example is the deposition of a molten droplet at temperature T_0 onto a semi-infinite, solid target at a temperature T_t below the melt's freezing point T_f (Fig. 1). If the scale is so small, or gravity so weak, that gravitational effects are negligible (small Bond number), and the deposition so gentle that the molten droplet does not break up upon impact (small or moderate Weber number), the droplet will typically spread in liquid form until the contact line is arrested by freezing, after which point the droplet's footprint will remain fixed, though the liquid above it may still undergo dynamic oscillations until solidification is complete. Since the subcooled target has an infinite thermal capacity, the final state will always be one where the deposited material is solid and at the target temperature.

The talk will describe three components of our work: (i) deposition experiments with small molten droplets, (ii) investigation of the dynamics of the molten contact line by means of a novel forced spreading method, and (iii) an attempt to provide a theoretical framework for answering the basic questions posed above.

(i) Deposition experiments were performed with molten droplets of waxes, water, and mercury. The thermal-dynamic scaling parameters for deposition are listed in Fig. 2, simplified to the case where the Weber number is small and the molten droplet and solid target are of the same material. Fig. 3 gives material properties and parameter values. The droplet radii ranged from 25 μm for the wax to about 300 μm for mercury and up to 1000 μm for water. Mercury was included because it possesses typical metal properties but, owing to its low melting point, is relatively free of interfacial oxidation problems. A high speed camera provided information on the global droplet dynamics during impact and spreading, including time scales and the final drop shape (Fig. 4 gives the ratio of the arrested footprint radius R^* and a , from which contact angle can be derived), but did not

give enough resolution to accurately determine dynamic contact angles during the spreading process.

(ii) To better investigate the contact line dynamics, we devised the forced spreading experiment shown schematically in Fig. 5. Using an apparatus similar to Gao & Sonin's (1994), a continuous stream of molten microdrops (radius 25 μm) is ejected at frequency f and ballistically delivered to a point on the target surface. The droplets coalesce as they arrive to form a sessile liquid macrodrop which grows and spreads laterally over the target. This simulates the spreading of a single, impacting droplet. The delivery frequency provides control over the contact line velocity $U=dR/dt$, where R is the macrodrop's contact line radius. The contact line motion can be filmed with a standard CCD camera through a microscope objective.

The video sequence of Fig. 6 shows a forced spreading experiment with molten wax on solid wax (only waxes have been studied with this technique so far). In the early stages the contact line moves much as it would for an ordinary liquid, and the relationship between θ and U is well represented by Hoffman's law with $\theta_e=0$. The contact line speed decreases as the macrodrop's base radius grows and, after the advance velocity slows to a critical value U^* , the contact line arrests rather abruptly at a radius R^* (Fig. 7). Our experiments show that U^* depends on target subcooling (Fig. 8), but is essentially independent of melt superheat $(T_0-T_f)/(T_f-T_l)$ and independent also of the macrodrop's spreading history (Fig. 8), which in this experiment is controlled via the delivery rate f and time. The primary parameter which determines U^* appears to be the Stefan number $S=c(T_f-T_l)/L$ based on target subcooling, c being the specific heat and L the latent heat. Contact line arrest is thus controlled mainly by processes near the contact line.

(iii) A freezing mechanism may be postulated based on the angle θ_s of the solidification front at the contact line (Fig. 9). A melt droplet will spread until the apparent liquid contact angle θ approaches θ_s , at which point the supply of melt to the contact line cannot be maintained and the spreading must stop. If this is correct, the melt's apparent contact angle θ will be given approximately by Hoffman's law with $\theta_e=0$ as long as $\theta_s \ll \theta$, and contact line freezing will occur when θ_s approaches θ . The arrest condition would therefore be obtained by calculating θ_s .

There is one problem with this: if we use the conventional continuum equations and boundary conditions (Fig. 10), the heat flux which controls the angle of the fusion interface is singular at the contact line (it has the same power-law form near the CL as Anderson & Davis's (1994) analysis for the purely conductive case). The angle θ_s cannot therefore be computed unless the continuum equations and/or boundary conditions are modified with a physically correct mechanism that removes the mathematical singularity.

The mechanism is at this time open to some speculation. Our first approach has been to ask whether a material can be characterized with a given cutoff length λ . We ask, at what distance from the contact line should the heat flux of the continuum solution be terminated to give a θ_s value in agreement with the experimental data for the arrest condition? Computations (Figs 10 and 11) show that the data for each of the three materials we have studied can indeed be adequately matched with a cut-off length λ , the value of which ranges from 0.08 to 0.3 μm depending on material (Fig. 12). These lengths are large compared with molecular scale, but smaller than the typical velocity slip lengths that have been used to fit continuum theories of the ordinary dynamic contact line to experimental data.

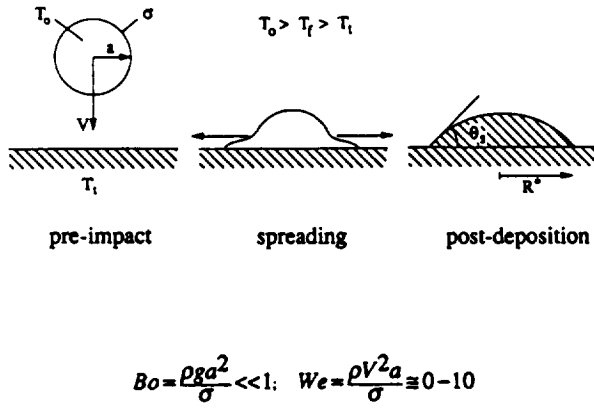
This research is at an early stage, and further work is required on both the experimental and theoretical sides to resolve the heat flux singularity and lay the basis for a complete theory of the molten contact line.

Acknowledgement: This work was supported by the National Science Foundation under Grants CTS-9122123 and CTS-9413026.

References

- D. M. Anderson and S. H. Davis, *JFM* **268** (1994) 231-265
- T. D. Blake and J. M. Haynes, *J. Colloid and Interface Sci.* **30** (1969) 421-423
- T. D. Blake and K. J. Ruschak, *Nature* **282** (1979) 489-491
- T. D. Blake, "Dynamic contact angles and wetting kinetics", in *Liquid Film Coating: Scientific Principles and their Technological Implications*, P. Schweitzer and S. Kistler, eds. Chapman, 1994.
- J. D. Chen and N. W. Wada, *J. Colloid and Interface Sci.* **148** (1992) 207-222
- R. G. Cox, *JFM* **168** (1986) 169-194
- P. G. de Gennes, *Rev. Mod. Phys.* **57** (1985) 827-863
- P. G. de Gennes, X. Hua and P. Levinson, *JFM* **212** (1990) 55-63
- P. A. Durbin, *JFM* **197** (1988) 157-169
- E. B. Dussan V. and S. H. Davis, *JFM* **65** (174) 71-95
- E. B. Dussan V., *JFM* **77** (1976) 665-684
- E. B. Dussan V., *Ann. Rev. Fluid Mechanics*, Vol. 11 (1979) 371-400
- E. B. Dussan V., E. Ramé and S. Garoff, *JFM* **230** (1991) 97-116
- M. Fermigier and P. Jenffer, *J. Colloid and Interface Sci.* **146** (1991) 226-241
- F. Gao and A. A. Sonin, *Proc. Royal Soc. London A* **444** (1994) 533-554
- E. V. Gribanova, *Advances in Colloid and Interface Science* **39** (1992) 235-255
- P. J. Haley and M. J. Miksis, *JFM* **223** (1991) 57-81
- L. M. Hocking, *JFM* **239** (1992) 671-681
- R. L. Hoffman, *J. Colloid and Interface Sci.* **50** (1975) 228-241
- C. Huh and L. E. Scriven, *J. Colloid and Interface Sci.* **35** (1971) 85-101
- J. Koplik and J. R. Banavar, *Ann. Rev. Fluid Mech.*, Vol 27 (1995) 257-292
- L. Leger and J. F. Joanny, *Reports on Progress in Physics* **55** (1992) 431-486
- C. G. Ngan and E. B. Dussan V. *JFM* **118** (1982) 27-40
- L. H. Tanner, *J. Phys. D.* **12** (1979) 1473-1484
- P. A. Thompson, W. B. Brinckerhoff & M. O. Robbins, *J. Adhesion Sci. Technol.* **7** (1993) 533-554

Fig. 1: Molten droplet deposition on subcooled solid of its own kind



Post-deposition droplet shape

- is not an equilibrium property (no equilibrium contact angle!)
- depends on thermal conditions and material properties

Fig. 2: Global scaling parameters for capillarity-driven droplet deposition

(We < 1)

$$Z = \frac{\mu}{\sqrt{\rho \sigma a}} = \text{Ohnesorge number}$$

$$\tau = \sqrt{\frac{\rho a^3}{\sigma}} = \frac{\text{time}}{\text{inertial/capillary timescale}}$$

$$S = \frac{c(T_f - T_i)}{L} = \text{Stefan number}$$

$$\beta = \frac{T_o - T_f}{T_f - T_i} = \frac{\text{melt superheat}}{\text{target subcooling}}$$

$$Pr = \frac{\nu}{\alpha} = \text{Prandtl number}$$

Π_j = additional parameters from quantities which characterize conditions at contact line

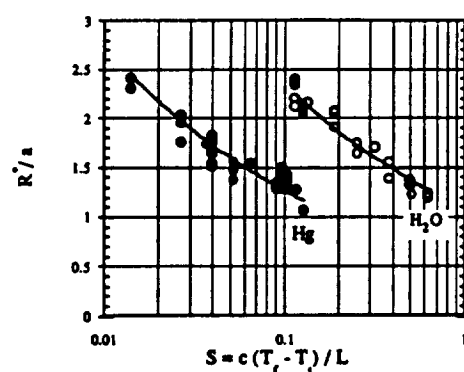
Fig. 3: Properties of Selected Materials

	α (m^2/s)	T_f (°C)	S @ $T_f - T_i = 10^\circ C$	Pr	Z @ $a = 100 \mu m$
Tin (3a)	4.0×10^{-5}	232	0.039	0.0065	3.2×10^{-3}
Tin 60-Lead 40 eutectic	3.3×10^{-5}	183	0.038	0.0077	3.1×10^{-3}
Mercury (Hg)	4.4×10^{-6}	-39	0.12	0.027	2.0×10^{-3}
Water (H_2O)	1.4×10^{-7}	0	0.13	7.0	1.2×10^{-3}
Microcrystalline wax	6.1×10^{-8}	91	0.11	300	3.6×10^{-1}

α = thermal diffusivity (m^2/s)

T_f = fusion temperature (°C)

Fig. 4: Effects of thermal conditions on final droplet shape



Final base radius R^*

- decreases with increasing target subcooling $S = c(T_f - T_i) / L$
- is insensitive to melt superheat $\beta = (T_o - T_f) / (T_f - T_i)$

Fig. 5: The forced spreading experiment

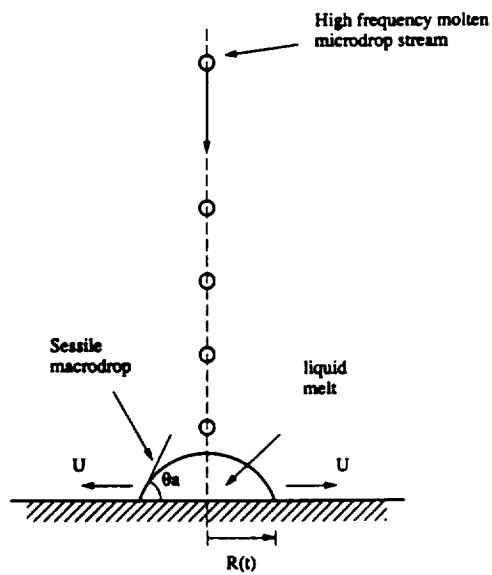
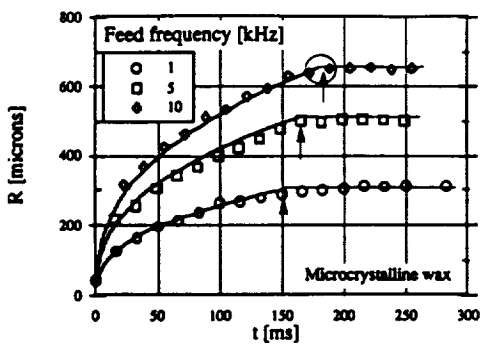


Fig. 7: Results from forced spreading experiments



Contact line arrest conditions (apparent contact angle θ_s and speed U^* just prior to arrest) are:

- (i) independent of macrodrop spreading history (i.e. no dependence on frequency of deposition)
- (ii) dependent on target subcooling

Fig. 6: Video sequence of forced spreading experiment. Microcrystalline wax, $T_0=117^\circ\text{C}$, $T_t=80^\circ\text{C}$, $T_f=91^\circ\text{C}$, $f=1\text{kHz}$, the rectangle's width is $100\ \mu\text{m}$

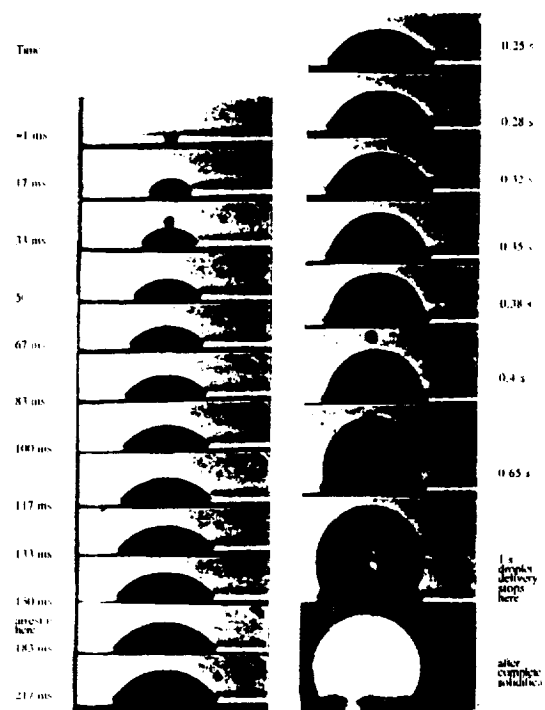


Fig. 8: CL speed just prior to arrest increases with target subcooling S and is independent of feed frequency f

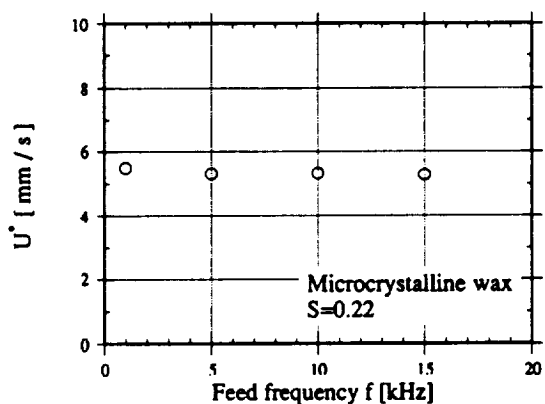
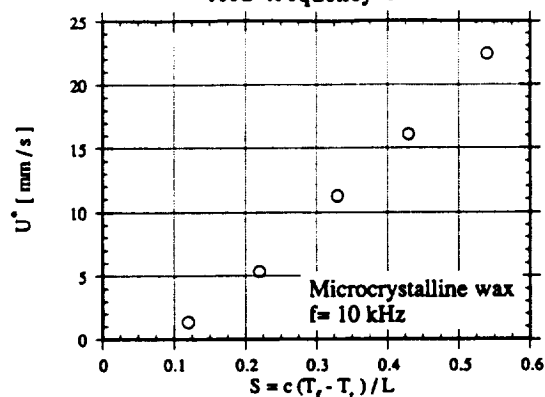


Fig. 9: The solidification front at the contact line

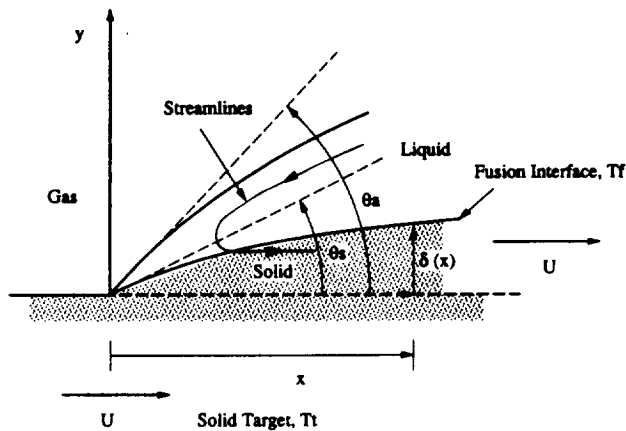


Fig. 10: Calculation of heat flux near the CL

Stefan condition: $\rho U L \sin \theta_s = q_s - q_l \approx q_s$:

$$\phi = \frac{T - T_i}{T_f - T_i}; \quad x = \frac{Ux}{\alpha}, \quad r = \frac{Uy}{\alpha}$$

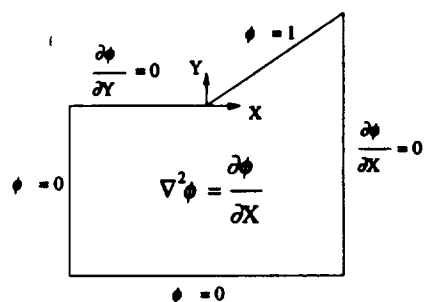


Fig. 11: Finite element calculation of temperature field for a wedge domain with $\theta = \pi/6$

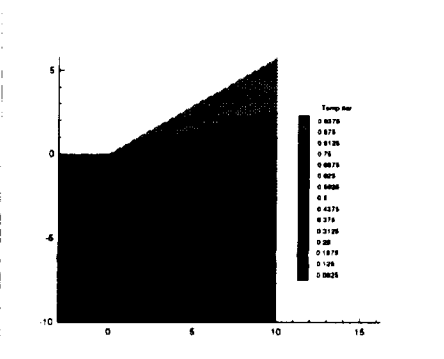
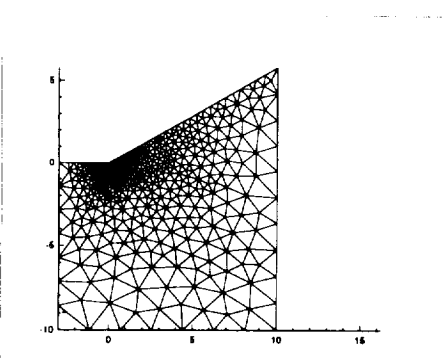


Fig. 12: Comparison of experiments and theory on molten contact line arrest

